Synthesis, structure and thermal behavior of volatile mononuclear mixed ligand complexes of rare-earth dipivaloylmethanates with diethylenetriamine

Albina Nikolaeva, Roy Nygaard, Irina Martynova, Dmitry Tsymbarenko *

Lomonosov Moscow State University, Moscow 119991, Russia

ARTICLE INFO

ABSTRACT

Highly volatile and stable complexes of rare-earth elements with mononuclear structure are of great importance for gas phase deposition of functional thin film materials. Mixed ligand complexes with β-diketonate anions (e.g. thd$^-$ = 2,2,6,6-tetrametylheptane-3,5-dionate) and ancillary neutral donor ligands demonstrate mononuclear structure and sufficient volatility, however, they are unstable to neutral ligand elimination especially in case of light rare earth elements. Here diethylenetriamine (deta) has been applied as tridentate neutral ligand to improve the stability of mixed ligand complexes due to macrochelate effect and additional weak intramolecular interactions, e.g. hydrogen bonds. Synthesis of a series of mixed-ligand [Ln(thd)$_3$(deta)], Ln = La (**1L**), Pr (**2L**), Nd (**3L**), Sm (**4L**) and Gd (**5L**) complexes, their X-ray single crystal structure characterization, DFT calculations, and thermal behavior study have been performed. Compounds **1L**-**5L** demonstrate similar mononuclear molecular structure, but different molecular packing of three types, which may undergo mutual transformation. Compounds **1L**-**4L** sublime intact in temperature range of 140–160 °C in vacuum without decomposition. **1L** was successfully applied as volatile precursors for MOCVD preparation of epitaxial complex oxide thin films, (*0 0 l*) LaMnO$_3$ and (*0 0 l*) LaAlO$_3$, on (*0 0 l*) MgO and (*0 0 l*) SrTiO$_3$ substrates.

1. Introduction

Nowadays rare earth elements (REE) are the most important components of thin-film functional materials which are widely used as superconductors [1,2], light emitters [3,4], multiferroics [5–9] and magnetic materials [10–12] etc. Metalorganic chemical vapor deposition (MOCVD) is one of the most universal and convenient method for producing such films, but it requires the development of volatile metal compounds, including REE [13,14]. The last ones are also important for gas phase isotope separation [15,16] (e.g. for radiopharmaceuticals [17]) and nuclear fission product separation [16]. All these applications require volatile mononuclear REE complexes with small molecular weight which are stable in the gas phase. Many types of REE metalorganic compounds were synthesized and among them complexes with β-diketonate anions (e.g. thd$^-$ = 2,2,6,6-tetrametylheptane-3,5-dionate, hfa$^-$ = 1,1,1,5,5,5-hexafluoro-2,4-pentanedionate) were found to be the most suitable [18,19]. However, REE ion in these compounds is expected to have coordination number equal to 6, which is insufficient for light REE. This leads to formation of polynuclear structures (e.g. dimeric [Ln(thd)$_3$]$_2$ [20]) or coordination of solvent molecules [21–23], which finally decreases the stability and volatility of compound. To overcome this obstacle, the mixed-ligand β-diketonate complexes Ln(β-dik)$_3$Q$_n$ with different N- and O-donor ligands were developed [19,24]. Among complexes with nonfluorinated β-diketones volatile mononuclear compounds Ln(thd)$_3$(phen) and Ln(thd)$_3$(bipy) with aromatic *N*-donor ligands (phen = 1,10-phenanthroline, bipy = 2,2′-bipyridine) were reported, while partial elimination of neutral ligand and π-π stacking interactions complicate their evaporation [19]. The complexes Ln(thd)$_3$Q, where Q is O-donor polyglyme ligands, which are free of π-π stacking, also split polyglyme in the gas phase [25]. Complexes with fluorinated β-diketones demonstrate higher volatility and better thermal stability [26,27]. However, their thermal decomposition in MOCVD process requires pyrohydrolysis to avoid the formation of fluorides. Therefore, the design of rare earth mixed-ligand complexes based on nonfluorinated β-diketones and aliphatic *N*-donor ligands is an actual task for development of highly volatile and stable against ligand elimination precursors for MOCVD.

For the light REE mixed-ligand complexes, tridentate diethylenetriamine (deta or dien) seems to be the most suitable neutral

* Corresponding author.
E-mail address: tsymbarenko@inorg.chem.msu.ru (D. Tsymbarenko).

ligand, since it allows to achieve the optimal CN equals to 9. Moreover, its flexibility makes it possible to fit variation in the ionic radius and NH_2 groups simultaneously with macrochelate effect may contribute to complex stabilization due to intramolecular hydrogen bonds. Indeed, REE mixed-ligand complexes with deta and even carboxylates or inorganic anions were reported to consist of isolated molecules [28–31]. However, no REE mixed-ligand β-diketonate complexes with deta have been reported till now.

Here, we report synthesis of a series of mixed-ligand [Ln(thd)₃(deta)] (**1L-5L**, Ln = La, Pr, Nd, Sm, Gd) complexes, their X-ray single crystal structures of three types, DFT calculations, thermal behavior and mutual transformations of different polytypes. Reported compounds demonstrate sufficient volatility and have been successfully applied as volatile precursors for MOCVD preparation of epitaxial $LaMnO_3$ and $LaAlO_3$ thin films on (0 0 l) MgO and (0 0 l) $SrTiO_3$ substrates.

2. Experimental

2.1. Starting materials and instrumentation

Chemically pure $Ln(NO_3)_3 \cdot 6H_2O$, KOH as well as ethanol (95%) purchased from local supplier (Reakhim, Russia), Hthd (98%, Dalchem) and deta (99%, Sigma-Aldrich) were used without further purification. [Mn(thd)₃] (**6**) and [Al(thd)₃] (**7**) were synthesized previously as described earlier and characterized by conventional methods [32–36].

C, H, N contents were determined by conventional elemental analysis using a Vario Micro Cube C, H, N analyzer (Elementar, Germany).

Ln content was determined gravimetrically, 50 mg of compound was placed into alundum crucible together with 150 mg of oxalic acid and was heat treated at 1000 °C for 1 h in air.

Thermogravimetric analysis was performed on Derivatograph Q-1500D (in air) with the rate of heating 10 °C/min. Weight of a sample is 50 mg. TG-DTA data are presented in the supplementary (Fig. S1).

IR spectra for solid state compounds in a form of powders were measured on a Perkin-Elmer Spectrum One FTIR spectrometer in ATR geometry in the range of 650–4000 cm^{-1}.

Powder XRD data were collected on a STOE Stadi P (curved Ge monochromator, $CuK\alpha_1$, λ = 1.540598 Å), Rigaku D/MAX and Rigaku SmartLab (graphite monochromator, CuKα) diffractometers. XRD patterns of thin films were recorded using Rigaku D/MAX 2500 and Rigaku Ultima IV (Cu anode, parallel beam optics, Eulerian cradle).

Single crystal X-ray diffraction data for **1**, **1L**, **4L** and **5L′** were collected on Bruker Smart APEX II diffractometer (MoKα radiation, graphite monochromator, λ = 0.71073 Å) and corrected for absorption by means of SADABS [37]. Data for single crystal of **7** was collected on XRD1 beamline of Elettra Synchrotron Facility (Trieste, Italy) with Dectris Pilatus 2 M detector using λ = 0.7000 Å radiation obtained by fixed exit double crystal Si (1 1 1) monochromator. The data were integrated and corrected for absorption by XDS software [38].

Magnetic behavior of **5L′** has been characterized by AC magnetic susceptibility measured by Quantum Design PPMS-9 in a temperature range of 2–300 K with 5Oe field oscillating at 337 Hz and zero permanent magnetic field (Fig. S2).

Chemical composition of thin films was characterized by ICP-MS analysis of solutions obtained by dissolving of thin films in nitric acid followed by proper dilution. Quadruple ICP-MS spectrometer Agilent 7500c (Agilent Technologies, Japan) with calibration solutions prepared from ICP-MS-68A (High-Purity Standards, USA) standard.

2.2. Preparation of [Ln(thd)₃]₂ (1–5)

KOH (8.58 mmol) and Hthd (10.72 mmol) were dissolved in water (50 mL) and ethanol (50 mL) mixture and dropwise added to $Ln(NO_3)_3$ (2.86 mmol) solution in water (50 mL) under vigorous stirring. The resulted mixture was stirred for 10 h and after that flaky precipitate was filtered off and dried in desiccator under reduced pressure. Final product was purified by preparative vacuum sublimation at 220 °C and 0.01 Torr similarly to **1L-5L** as described in section 2.4. Yield is 90–95%.

2.2.1. [La(thd)₃]₂ (1)
Anal. calc. for $LaC_{33}O_6H_{57}$ (%): La, 20.17; C, 57.55; H, 8.34. Found (%): La, 19.79, C, 57.86; H, 8.25. IR (ν, cm^{-1}): 2955, 2929, 2905, 2870 ν(C—H); 1571, 1539 $ν_{as}$(C═O); 1505, 1453, 1408 $ν_s$(C═O); 1388, 1359, 1282, 1246, 1226.

2.2.2. [Pr(thd)₃]₂ (2)
Anal. calc for $PrC_{33}O_6H_{57}$ (%): Pr, 20.4; C, 57.38; H, 8.32. Found (%): Pr, 20.47; C, 57.51; H, 8.20. IR (ν, cm^{-1}): 2955, 2929, 2905, 2870 ν(C—H); 1571, 1539 $ν_{as}$(C═O); 1505, 1453, 1408 $ν_s$(C═O); 1388, 1359, 1282, 1246, 1226.

2.2.3. [Nd(thd)₃]₂ (3)
Anal. calc. for $NdC_{33}O_6H_{57}$ (%): Nd, 20.78; C, 57.11; H, 8.28. Found (%): Nd, 21.05; C, 57.15; H, 8.23. IR (ν, cm^{-1}): 2955, 2929, 2905, 2870 ν(C—H); 1571, 1539 $ν_{as}$(CO); 1505, 1453, 1408 $ν_s$(C═O); 1388, 1359, 1282, 1246, 1226.

2.2.4. [Sm(thd)₃]₂ (4)
Anal. calc. for $SmC_{33}O_6H_{57}$ (%): Sm, 21.47; C, 56.61; H, 8.21. Found (%): Sm, 21.12; C, 55.99; H, 8.14. IR (ν, cm^{-1}): 2952, 2904, 2867 ν(C—H); 1569, 1537 $ν_{as}$(C═O); 1495, 1450, 1397 $ν_s$(C═O); 1382, 1354, 1282, 1246, 1224.

2.2.5. [Gd(thd)₃]₂ (5)
Anal. calc. for $GdC_{33}O_6H_{57}$ (%): Gd, 22.24; C, 56.06; H, 8.13. Found (%): Gd, 21.29; C, 56.03; H, 8.08. IR (ν, cm^{-1}): 2955, 2929, 2905, 2870 ν(C—H); 1571, 1539 $ν_{as}$(C═O); 1505, 1453, 1408 $ν_s$(C═O); 1388, 1359, 1282, 1246, 1226.

2.3. Preparation of Ln(thd)₃(deta) (1L-5L, 2L′, 5L′)

Thin powder of complexes **1–5** (2 mmol) was suspended in EtOH (50 mL) at 50 °C, then deta was dropwise added (3 mmol) and mixture was left under vigorous stirring for 2 h at room temperature. Two different techniques were used to isolate the product. Precipitates of **1L-5L** were filtered off at 25 °C and washed by 1 mL of ethanol. Alternatively, to get **2L′**, **5L′** reactive mixture was left to evaporate under heating at 70 °C to ca. 10% of original volume with the following filtration of resulting precipitates.

2.3.1. La(thd)₃(deta) (1L)
Anal. calc. for $LaC_{37}O_6N_3H_{70}$ (%): La, 17.54; C, 56.12; H, 8.91; N, 5.31. Found (%): La, 16.75; C, 55.70; H, 9.05; N, 5.24; IR (ν, cm^{-1}): 3374, 3304, 3275 ν(N—H); 2951, 2901, 2870 ν(C—H); 1584, 1574 $ν_{as}$(C═O); 1533, 1502, 1449 $ν_s$(C═O); 1412, 1385, 1356, 1278, 1225.

2.3.2. Pr(thd)₃(deta) (2L)
Anal. calc. for $PrC_{37}O_6N_3H_{70}$ (%): Pr, 17.75; C, 55.98; H, 8.89; N, 5.29. Found (%): Pr, 17.81; C, 55.93; H, 8.81; N, 5.21. IR (ν, cm^{-1}): 3388, 3316, 3285 ν(N—H); 2949, 2901, 2870 ν(C—H); 1585, 1573 $ν_{as}$(C═O); 1533, 1502, 1449 $ν_s$(C═O); 1401, 1385, 1354, 1279, 1226.

2.3.3. Pr(thd)₃(deta) (2L′)

Anal. calc. for $PrC_{37}O_6N_3H_{70}$ (%): Pr, 17.75; C, 55.98; H, 8.89; N, 5.29. Found (%): Pr, 18.01; C, 55.87; H, 8.78; N, 5.42. IR (ν, cm⁻¹): 3387, 3317, 3286 ν(N—H); 2950, 2900, 2864 ν(C—H); 1585, 1572 $ν_{as}$(C⸻O); 1533 , 1502, 1449 $ν_s$(C⸻O); 1402, 1385, 1355, 1280, 1225.

2.3.4. Nd(thd)₃(deta) (3L)

Anal. calc. for $NdC_{37}O_6N_3H_{70}$ (%): Nd, 18.09; C, 55.74; H, 8.85; N, 5.27. Found (%): Nd, 18.44; C, 55.86; H, 8.74; N, 5.25. IR (ν, cm⁻¹): 3382, 3305, 3276 ν(N—H); 2950, 2901, 2867 ν(C—H); 1584, 1574 $ν_{as}$(C⸻O); 1533, 1503, 1449 $ν_s$(C⸻O); 1413, 1385, 1356, 1279, 1225.

2.3.5. Sm(thd)₃(deta) (4L)

Anal. calc. for $SmC_{37}O_6N_3H_{70}$ (%): Sm, 18.72; C, 55.32; H, 8.78; N, 5.23. Found (%): Sm, 19.78; C, 55.28; H, 9.05; N, 5.31. IR (ν, cm⁻¹): 3390, 3315, 3285 ν(N—H); 2950, 2901, 2865 ν(C—H); 1586, 1574 $ν_{as}$(C⸻O); 1533, 1503, 1449 $ν_s$(C⸻O); 1404, 1385, 1354, 1279, 1226.

2.3.6. Gd(thd)₃(deta) (5L)

Anal. calc. for $GdC_{37}O_6N_3H_{70}$ (%): Gd, 19.41; C, 54.85; H, 8.71; N, 5.19. Found (%): Gd 19.92; C, 55.05; H, 8.87; N, 5.23. IR (ν, cm⁻¹): 3388, 3316, 3288 ν(N—H); 2951, 2902, 2867 ν(C—H); 1588, 1574 $ν_{as}$(C⸻O); 1537, 1505, 1450 $ν_s$(C⸻O); 1411, 1386, 1356, 1282, 1226.

2.3.7. Gd(thd)₃(deta) (5L′)

Anal. calc. for $GdC_{37}O_6N_3H_{70}$ (%): Gd, 19.41; C, 54.85; H, 8.71; N, 5.19. Found (%): Gd, 19.45; C, 54.82; H, 8.78; N, 5.15. IR (ν, cm⁻¹): 3404, 3389, 3316 ν(N—H); 2950, 2902, 2865 ν(C—H); 1587, 1573 $ν_{as}$(C⸻O); 1533, 1503, 1450 $ν_s$(C⸻O); 1425, 1406, 1386, 1355, 1226.

2.4. Preparative vacuum sublimation

The portion of **1L-5L** or **2L′** powder (100 mg) in quartz boat was placed into glass tube, evacuated and retained at 140–160 °C for one hour under pressure of 10^{-2} torr. Sublimation products **1L-subl**-**5Lsubl** and **2L′subl**, which condensed in the cold part of the glass tube, were collected and characterized. The CHN and IR data are presented in supplementary (Table S1).

2.5. X-ray crystallography

Single crystals of compounds **1**, **1L**, **4L**, **5L′** and **7** suitable for analysis were obtained by the slow crystallization of mother liquors (**1L**, **4L**, **5L′**) or by recrystallization from benzene (**1**) or toluene (**7**) solution. The structures were solved by direct methods and refined by full-matrix least squares on |F²| with anisotropic thermal parameters for all non-hydrogen atoms except structure **5L′**, where only Gd atoms were treated anisotropically. The positions of hydrogen atoms were calculated geometrically and refined in the riding model with fixed isotropic thermal parameters. All calculations were performed using the SHELXTL PLUS 5.0 program package [39]. The essential crystallographic parameters are summarized in Table 1.

2.6. Quantum chemical calculations

Theoretical simulations were performed for isolated molecules with the FireFly 8.2 program package [40] in the framework of Density Functional Theory (PBE0 functional). Geometry optimization and vibration frequencies calculations were performed using the 6-31G(d) basis sets for C, O, N and H atoms, while for total

energy calculations extended 6-311+G(d, p) were applied. The quasi-relativistic Stuttgart-Cologne effective core potentials were used for La (ECP46MWB), Sm (ECP51MWB) and Gd (ECP53MWB) with the corresponding basis sets [41]. The geometries of the molecules were optimized without symmetry restraints and were checked for the absence of imaginary frequencies in the Hessian. The thermodynamic functions of the modeling reactions were calculated as follows:

$$\Delta_r E = \sum \left(E_{products} \right) - \sum \left(E_{reactants} \right) - \Delta E_{BSSE} \tag{1}$$

$$\Delta_r H^{298} = \Delta_r E + \sum \left(H^{298}_{products} \right) - \sum \left(H^{298}_{reactants} \right) \tag{2}$$

$$\Delta_r S^{298} = \sum \left(S^{298}_{products} \right) - \sum \left(S^{298}_{reactants} \right) \tag{3}$$

$$\Delta_r G^T = \Delta_r H^{298} - T\Delta_r S^{298} \tag{4}$$

where E_i is the full DFT energy of molecule calculated in the extended basis set, ΔE_{BSSE} is the correction for basis set superposition error calculated by the Boys and Bernardi approach [42]. The values of H_i, the non-electronic contribution to full enthalpy, and S_i, the entropy of the molecule, were obtained in the model of harmonic oscillator – rigid rotators. $\Delta_r H^{298}$ and $\Delta_r S^{298}$ were considered to be constant in temperature range 298–433 K. The optimized molecules, along with the geometrical parameters and are listed in the supplementary (Table S2).

2.7. Thin film deposition

The deposition of $LaMnO_3$ and $LaAlO_3$ thin films on single crystalline (0 0 1) MgO and (0 0 1) $SrTiO_3$ substrates was performed using hot-wall MOCVD reactor with a single flash-evaporator described elsewhere [43], which was loaded by a mixture of volatile precursors of certain composition. Powders of **1** or **1L** were used as volatile precursors of La, while well-known volatile [Mn(thd)₃] (**6**) and [Al(thd)₃] (**7**) were precursors of Mn and Al respectively. Composition of precursors mixture, namely La:Mn or La:Al ratio, was optimized in the range of 0.5–2.0 to obtain stoichiometric single-phase films. The following conditions were applied for all MOCVD experiments: evaporator temperature – 200 °C and feeding rate – 2 mg/min, the oxygen partial pressure – 2 mbar and the total gas pressure – 4.7 mbar. The substrate temperature was 750 °C for $LaMnO_3$ and 900 °C for $LaAlO_3$ layers deposition.

3. Results and discussion

3.1. Synthesis

Synthesis and thermal behavior of whole row of REE dipivaloylmethanates were widely studied earlier [20,25,44–46]. For light REE [Ln(thd)₃]₂ complexes the crystal structure of [Pr(thd)₃]₂ at room temperature and [Ln(thd)₃]₂ (Ln = La-Gd) at 150 K have been reported recently to be isostructural [20,25,44–46]. In the present work, we have prepared **1–5** as intermediates for the further synthesis, purified them by vacuum sublimation and confirmed their identity by CHN, IR and XRD, which data are in good agreement with previously reported ones [45]. It was, surprisingly, observed that just-obtained **1** sublimate shows XRD pattern which differs from theoretical one of **1** (Fig. S3). However, XRD pattern of **1** sublimate after storage in air becomes similar to theoretical one of **1** and experimental patterns of **2–5**. This behavior points to the condensation of polymorphous metastable phase of "La(thd)₃" from vapor which rapidly transforms to stable structure **1**. Attempts to grow the X-ray quality single crystal of this

Table 1
Crystallographic and refinement data for structures **1**, **1L**, **4L**, **5L′** and **7**.

| Parameters	1	1L	4L	5L′	7
Formula	La$_2$C$_{66}$O$_{12}$H$_{114}$	LaC$_{37}$O$_6$N$_3$H$_{70}$	SmC$_{37}$O$_6$N$_3$H$_{70}$	GdC$_{37}$O$_6$N$_3$H$_{70}$	AlC$_{33}$O$_6$H$_{57}$
Formula weight	1377.39	791.87	803.31	810.21	576.77
T(K)	100(2)	120(2)	120(2)	120(2)	100(2)
Crystal system	Monoclinic	Orthorhombic	Triclinic	Triclinic	Monoclinic
Space group	P 2$_1$/n	Pnma	P1$^-$	P1$^-$	C 2/c
a, Å	12.3908(8)	17.1955(8)	10.925(4)	10.94(3)	28.0303(3)
b, Å	27.8470(16)	24.9221(12)	11.259(4)	23.49(6)	18.42055(16)
c, Å	21.8074(14)	10.1925(5)	19.004(7)	26.07(6)	21.4456(2)
α, (°)	90.00	90.00	95.102(9)	73.56(3)	90.00
β, (°)	105.1318(13)	90.00	105.974(8)	89.15(3)	98.0185(9)
γ, (°)	90.00	90.00	103.727(8)	87.62(3)	90.00
V, Å^3	7263.7(8)	4368.0(4)	2153.2(14)	6417(26)	10964.84(18)
Z	4	4	2	6	12
Color, habit	Colorless, prism	Colorless, plate	Colorless, block	Colorless, block	Colorless, block
Crystal dimensions, mm	0.40 × 0.20 × 0.20	0.40 × 0.20 × 0.05	0.15 × 0.14 × 0.12	0.03 × 0.02 × 0.01	0.16 × 0.07 × 0.07
D$_{calc}$, g cm^{-3}	1.260	1.204	1.239	1.258	1.048
μ, mm^{-1}	1.213	1.019	1.405	1.592	0.092
Unique reflections (R$_{int}$)	17493(0.0471)	6508(0.0588)	9358(0.0750)	8173(0.3390)	12432(0.0248)
Observed reflections [I > 2σ(I)]	13,105	4960	7130	2809	10,886
Parameters	772	303	442	668	570
R$_1$[I > 2σ(I)], ωR$_2$	0.0498, 0.1060	0.0373, 0.0860	0.0551, 0.1112	0.1531, 0.3339	0.0626, 0.1798
Goodness-of-fit (GOF) on F^2	1.064	1.100	0.997	1.018	1.033
Absorption correction	SADABS	SADABS	SADABS	SADABS	XDS
T$_{min}$, T$_{max}$	0.643, 0.793	0.694, 0.887	0.753, 0.862	0.960, 0.980	0.847, 0.994
ρ$_{min}$, ρ$_{max}$, e Å^{-3}	−0.990, 1.245	−1.822, 2.143	−1.622, 0.952	−1.381, 0.966	−0.464, 0.648

metastable phase from the vapor were not successful, while recrystallization of sublimate from benzene solution led to single crystal of stable phase **1**.

Mixed ligand complexes **1L-5L** were synthesized by direct interaction between preliminary obtained **1–5** and deta in organic medium. Compounds **1–5** being nonpolar are highly soluble in nonpolar solvents (for example, toluene, benzene) [47], which are not compatible for synthesis with polar deta ligand. Therefore, we used ethanol as solvent for synthesis, where deta dissolves completely and **1–5** demonstrate moderate solubility. As a result of heterogeneous reaction, we observed transformation of undissolved residue from loose to crystalline precipitate. The last one was isolated by filtration in two ways: (i) just after synthesis at 25 °C of **1L-5L**; (ii) after solvent evaporation under heating at 70 °C to ca. 10% of original volume (**2L′**, **5L′**) (Scheme 1). The products were examined by TGA, CHN analyses, IR spectroscopy that

show their composition to be of general formula [Ln(thd)$_3$(deta)] regardless of method of isolation. Moreover, no changes in composition were observed with increase of deta : [Ln(thd)$_3$] ratio in synthetic mixture up to 3:1.

However, despite their identical composition compounds **1L-5L**, **2L′**, **5L′** demonstrate polymorphism, powder XRD data show them to belong to 3 structural types: type I – **1L**, **3L**; type II – **2L**, **4L**, **5L**; type III – **2L′**, **5L′**. Each type was characterized by single crystal XRD for crystals of **1L**, **4L**, **5L′** and comparison between experimental and theoretical XRD patterns (Figs. 1, S4).

This polymorphism of [Ln(thd)$_3$(deta)] and [La(thd)$_3$]$_2$ as well, originates from structural flexibility of lanthanides' coordination sphere, bulky *tert*-butyl substituents of thd$^-$ and absence of specific intermolecular interactions. It could make impact on structure related properties (e.g. volatility) of compounds and their reliable identification requires XRD analysis.
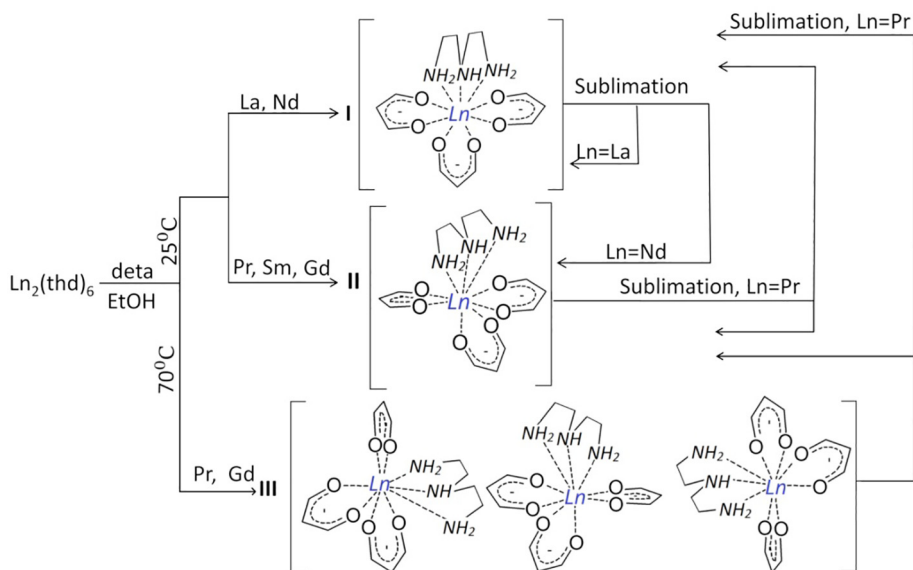
Scheme 1. The obtaining of mixed-ligand complexes of various structural types I-III and their mutual transformations.
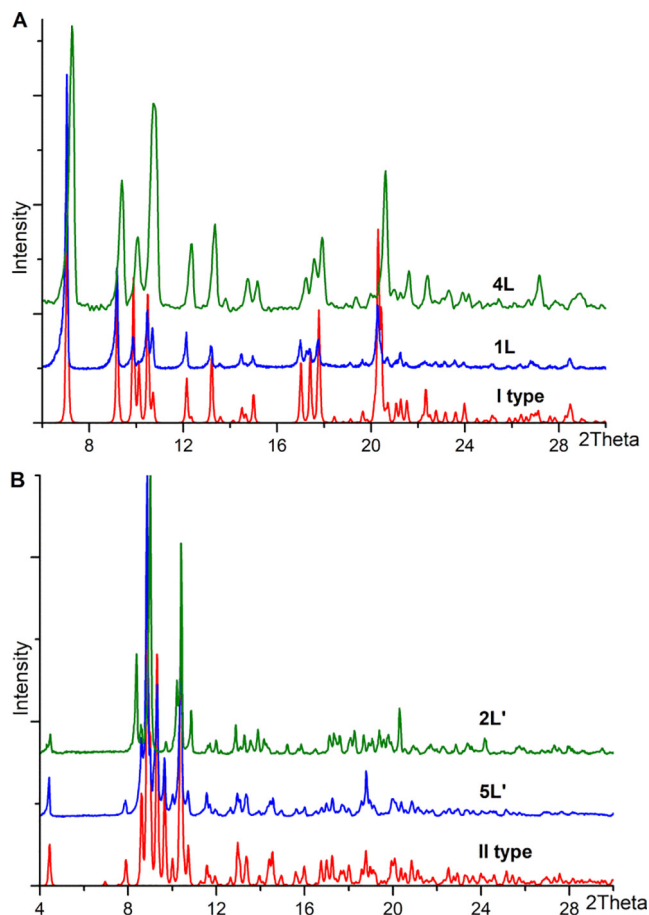
Fig. 1. Powder XRD patterns of [Ln(thd)₃(deta)] compounds of different structural types: a) type I, experimental patterns of **1L**, **3L** and theoretical one (lower line); b) type III, experimental patterns for **2L′**, **5L′** and theoretical one (lower line). Theoretical patterns were calculated basing on **1L** and **5L′** structures which were corrected for thermal expansion with the following unit cell parameters: **1L**: *Pnma*, a = 17.478(4) Å, b = 25.053(5) Å, c = 10.417(2) Å ; **5L′**: *P1̄*, a = 11.211(11) Å, b = 23.750(19) Å, c = 26.50(3) Å, α = 74.13(7)°, β = 88.87(7)°, γ = 86.46(8)°.

3.2. X-ray crystal structures

3.2.1. [La(thd)₃]₂ (**1**) and [Al(thd)₃] (**7**)

Monoclinic unit cell of **1** contains 4 symmetry related isolated binuclear pseudo centrosymmetric molecules. Each molecule contains La1 and La2 ions in seven-fold coordination, four chelating and two chelate-bridging thd⁻ ligands (Fig. 2). La1 and La2 demonstrate similar distorted one-capped trigonal prism coordination environment with differences in corresponding La-O distances (Table S3). The isolated molecules are packed in the crystal without any specific interactions. Molecular geometry of [La(thd)₃]₂ at 100 K is very close to one at 150 K reported in [45], with corresponding Ln-O distances being by 0.01–0.03 Å shorter.

Crystal structure of **7** has been recently studied in terms of polymorphism [36]. Two polymorphous modifications – monoclinic in *C2/c* (at 293 K and 150 K) and triclinic in *P1⁻* (at 293 K) have been reported [34–36]. It is worth noting, that molecular volume, which serves as a measure of packing efficiency, reveals the difference in relative stability of polymorphs [48], namely the lower volume most probably corresponds to more favorable polymorph. Triclinic phase demonstrates molecular volume of 923 Å³, which is lower than respective values for monoclinic one at 293 K (967 Å³) and even at 150 K (928 Å³). Here we have performed structural determination of **7** at 100 K (Fig. S5) and it also exhibits monoclinic symmetry with the lowest value of molecular
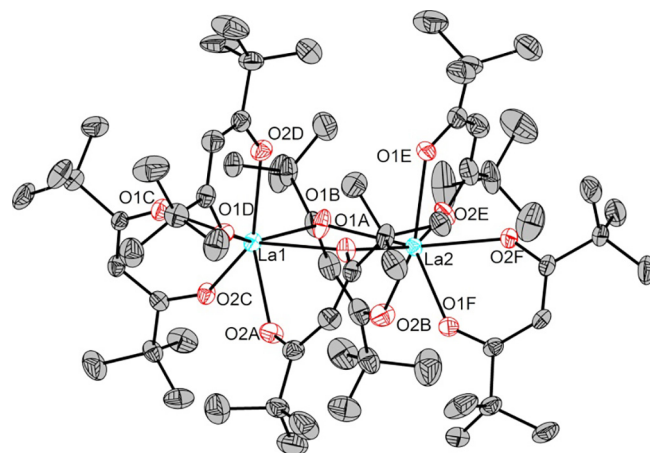
Fig. 2. Geometry of [La(thd)₃]₂ molecule in structure **1**.

volume (914 Å³). Therefore no thermal induced phase transition between two polymorphs occurs in 100–293 K temperature range, and monoclinic phase seems to be the low-temperature modification which is metastable at room temperature. Comparison of Al-O interatomic distances in structures which have been reported earlier with one reported here reveals minor variations (Table S4).

3.2.2. [La(thd)₃(deta)] (**1L**)

Orthorhombic unit cell of **1L** represents the structural type I and contains 4 symmetry related isolated mononuclear [La(thd)₃(-deta)] molecules with central ions lying in a special *m* position. Central ion La1 coordinates four O atoms (O1, O2, O1ⁱ and O2ⁱ) of two symmetry related chelating thd⁻, two O atoms (O3 and O3ⁱ) of chelating thd⁻ lying across *m*-plane and three N atoms of bichelating deta, which are disordered over two positions with equal occupancies (Table 2). The coordination environment of La1 is best described as one-capped square antiprism with CN equals to 9 (Fig. 3).

Neighbor molecules in **1L** are arranged in closest packing motif and surprisingly exhibit no hydrogen bonds (Fig. S6A). However, slight electrostatic interactions between NH₂ groups of deta and conjugated system of thd⁻ cause arrangement of molecules into chains along *a* axis with La1···La1ⁱⁱ separation being equal to 8.9311 (4) Å.

3.2.3. [Sm(thd)₃(deta)] (**4L**)

Structure **4L** represents the structural type II. Asymmetric part of triclinic unit cell contains one [Sm(thd)₃(deta)] molecule. Central ion Sm1 coordinates six O atoms of chelating thd⁻ and three N atoms of bichelating deta. In contrast to **1L** the coordination environment of Sm1 is best described as three-capped trigonal prism with CN equals to 9 (Fig. 4).

The isolated molecules Sm(thd)₃(deta) in **4L** form layers arranged in closest packing motif with the closest Sm1···Sm1 (1 − x, 1 − y, 1 − z) separation within the layer being equal to 8.455(3) Å and no intermolecular hydrogen bonds similar to **1L** (Fig. S6B).
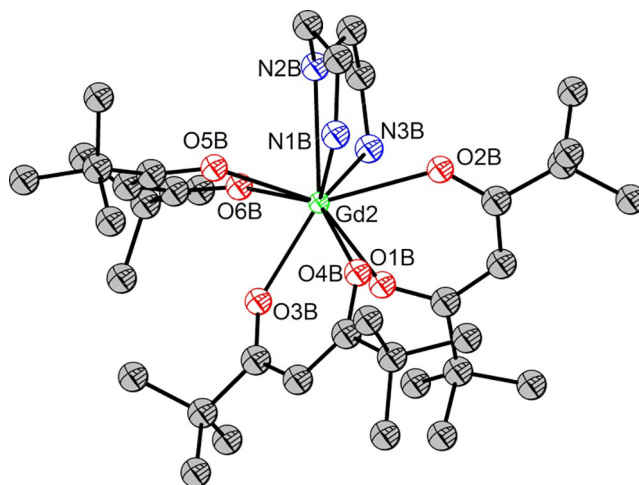
3.2.4. [Gd(thd)₃(deta)] (**5L′**)

The best single crystal of **5L′** demonstrates drastic decay of diffraction spots' intensity with increase of diffraction angle, almost no reflections with I > 2σ(I) were observed at 2θ > 34° even with 70 s per frame acquisition time at 120 K. This behavior originates from low lattice energy and weak ordering of bulky molecules of **5L′** and prevents precise determination of unit cell parameters and atomic coordinates. However, the independent

Table 2
Bond distances for [La(thd)$_3$(deta)] (**1L**), [Sm(thd)$_3$(deta)] (**4L**) and [Gd(thd)$_3$(deta)] (**5L′**).

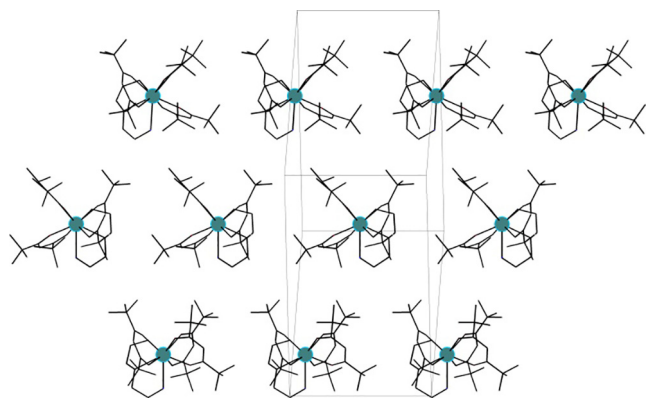|	**1L**	**4L**	**5L′**		
			5L′A	5L′B	5L′C
Bond distances, Å					
Ln1-O1	2.447(2)	2.371(4)	2.26(2)	2.31(3)	2.34(2)
Ln1-O2	2.5376(18)	2.456(4)	2.42(3)	2.44(3)	2.40(3)
Ln1-O3	2.482(2)	2.381(4)	2.34(2)	2.25(2)	2.33(3)
Ln1-N1	2.732(4)	2.619(4)	2.57(4)	2.61(4)	2.63(4)
Ln1-N2	2.754(4)	2.675(5)	2.54(4)	2.65(5)	2.61(5)
Ln1-N3	2.716(4)	2.671(4)	2.60(4)	2.56(4)	2.63(4)
Ln1-O4 (La1-O3^i)	2.482(2)	2.380(3)	2.33(3)	2.26(3)	2.31(2)
Ln1-O5 (La1-O1^i)	2.447(2)	2.427(4)	2.28(2)	2.32(2)	2.36(2)
Ln1-O6 (La1-O2^i)	2.5377(18)	2.417(3)	2.40(3)	2.33(2)	2.38(2)
Average distances, Å					
Ln-O$_{thd}$	2.49 ± 0.04	2.41 ± 0.03	2.34 ± 0.06	2.32 ± 0.07	2.35 ± 0.03
Ln-N$_{deta}$	2.73 ± 0.02	2.66 ± 0.03	2.57 ± 0.03	2.61 ± 0.05	2.62 ± 0.01

Symmetry code: (i) x, 1.5-y, z.
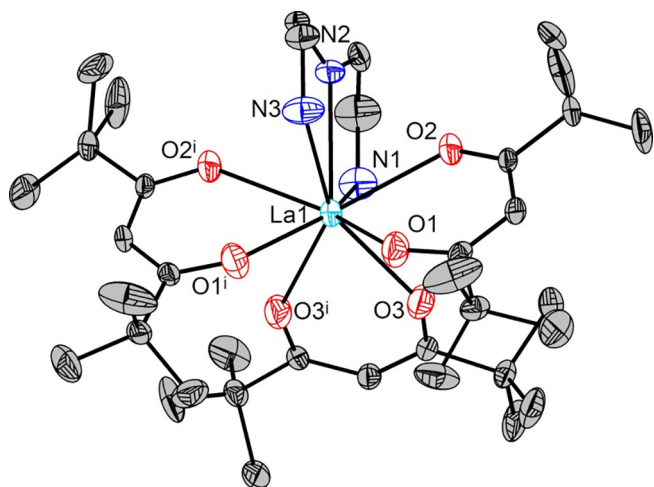
Fig. 3. Geometry of La(thd)$_3$(deta) molecule in **1L** structure. Hydrogen atoms are omitted for clarity.
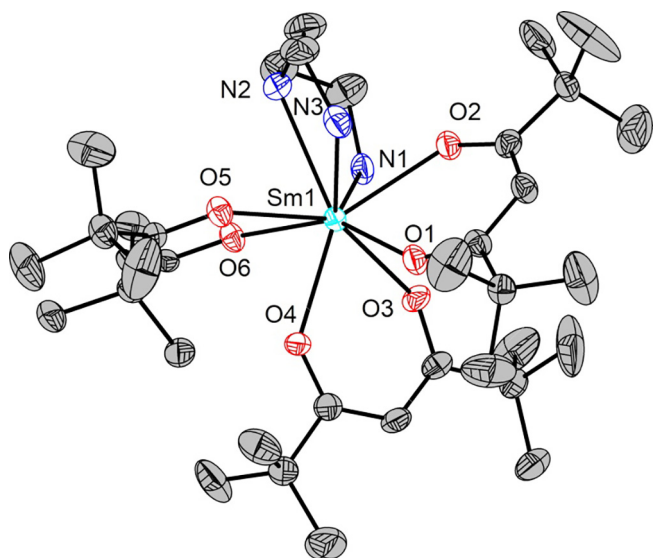
Fig. 4. Geometry of Sm(thd)$_3$(deta) molecule in **4L** structure. Hydrogen atoms are omitted for clarity.

indexing of powder XRD pattern of **5L′** (Fig. 1B) confirms single crystal data and makes it possible to rely on refined structure.

Structure **5L′** represents the structural type III. Asymmetric part of triclinic unit cell of **5L′** contains three molecules, **5L′**A, **5L′**B, **5L′**C respectively, with geometry being similar to each other and to one in **4L**. Each central Gd ion coordinates six O atoms of chelating thd$^-$ and three N atoms of bichelating deta. The coordination environment of Gd is best described as three-capped trigonal prism with CN equals to 9 similar to **4L** (Fig. 5). Two thd$^-$ ligands in **5L′**A are disordered over two positions with equal occupations, retaining the coordination environment of Gd unchanged.

The isolated molecules in **5L′** form pseudo-hexagonal layers parallel to (0 1 1) lattice plane (Fig. 6). In contrast to **1L** and **4L** these layers are arranged with alternation of the closest packing and simple packing motif. The shortest intermetallic distance, Gd2···Gd3, equals to 9.454(18) Å.

Therefore, compounds **1L**, **4L**, **5L′** demonstrate equal CN of central ion, but different coordination environment. The average Ln-O and Ln-N distances decrease along with ionic radius (Table 3), being close to the respect values, 2.38 ± 0.04, 2.65 ± 0.04 Å, in [Eu(thd)$_3$(terpy)] which is the only Ln(thd)$_3$Q mixed ligand complex with tridentate N-donor ligand to the best of our knowledge (terpy = 2,2′:6′,2″-Terpyridine) [49]. Moreover, the Ln polyhedron in **4L**, **5L′**, being a distorted three-capped trigonal prism, is similar to one in [Eu(thd)$_3$(terpy)]. No Ln(thd)$_3$Q structures with the

Fig. 5. Geometry of Gd(thd)$_3$(deta) molecule in **5L′** structure. Hydrogen atoms are omitted for clarity.

Fig. 6. Arrangement of Gd(thd)₃(deta) molecules within pseudo-hexagonal layer parallel to (0 1 1) lattice plane in **5L′** structure. Hydrogen atoms are omitted for clarity.

Table 3
DFT calculated thermodynamic data for reactions (7)-(9).

Parameter	Ln = La	Ln = Sm	Ln = Gd
Ln(thd)₃(g) → ½ Ln₂(thd)₆(g) (7)			
ΔE, kJ/mol	−90.0	−87.2	−86.1
ΔH, kJ/mol	−87.5	−84.4	−83.2
ΔS, J/(mol·K)	−214	−207	−210
ΔG²⁹⁸, kJ/mol	−23.6	−22.6	−20.7
ΔG⁴³³, kJ/mol	5.3	5.3	7.7
Ln(thd)₃(deta)(g) → Ln(thd)₃(g) + deta(g) (8)			
ΔE, kJ/mol	189.9	181.1	181.4
ΔH, kJ/mol	156.3	146.2	146.7
ΔS, J/(mol·K)	292	294	287
ΔG²⁹⁸, kJ/mol	69.2	58.6	61.0
ΔG⁴³³, kJ/mol	29.7	19.0	22.3
Ln(thd)₃(deta)(g) → ½ Ln₂(thd)₆(g) + deta(g) (9)			
ΔH, kJ/mol	68.8	61.8	63.5
ΔS, J/(mol·K)	78	87	77
ΔG²⁹⁸, kJ/mol	45.6	36.0	40.4
ΔG⁴³³, kJ/mol	35.0	24.3	29.9

aliphatic tri- or higher dentate *N*-donor ligands have been reported till now, while there are few with related O-donor ligands – polyglymes. CN being equal to 9 has been reported only for [La(thd)₃(tetraglyme)] [50], but CN equals to 8 in [Eu₂(thd)₆(triglyme)] [50] and [Gd₂(thd)₆(tetraglyme)] [51]. While in Ln(hfa)₃(polyglyme), where hfa is hexafluoroacetylacetonate anion which promotes stronger Ln- polyglyme interaction, each Ln = La-Tb binds three O-atoms of polyglyme with the resulting CN equals to 9 [26,27,52,53]. Therefore, compounds **1L-5L, 2L′, 5L′** are expected to demonstrate the stability against ligand elimination similar to Ln(hfa)₃(polyglyme) analogues rather than Ln(thd)₃(polyglyme).

3.3. Thermal behavior in vacuum

Behavior of mixed-ligand complexes **1L-5L** and **2L′** were examined in 140–160 °C temperature range by preparative vacuum evaporation. It was observed that all compounds evaporate rapidly and with no remarkable nonvolatile residue left. Volatile products after condensation in the cold part of vacuum vessel were collected as crystalline powders **1Lsubl-5Lsubl**, and **2L′subl**. According to CHN and IR data (Table S1) the compounds after sublimation, **1Lsubl-4Lsubl**, **2L′subl**, demonstrate unchanged composition of general formula [Ln(thd)₃(deta)]. While [Gd(thd)₃(deta)] compound, **5L**, partially decomposed during evaporation and **5Lsubl** demonstrated reduced deta content.
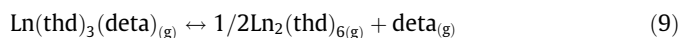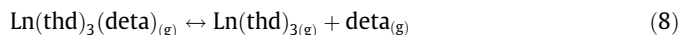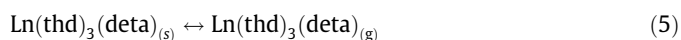
Nevertheless, despite identical chemical composition **1Lsubl-4Lsubl** and **2L′subl** contain crystalline phases of different

structural types. Namely, **1Lsubl** contains [Ln(thd)₃(deta)] of type I; **2Lsubl** and **2L′subl** – the mixture of types I and II; **3Lsubl** – type II; and **4Lsubl** – the mixture of types I and III (Fig. 7).

3.4. DFT calculations

Since [Ln₂(thd)₆] and [Ln(thd)₃(deta)] molecules are considered as volatile compounds, it is important to study their molecular structure in the gas phase, as well as their stability and transformations at moderate temperatures (413–523 K). Therefore, we have performed DFT calculations of three series of molecules [Ln₂(thd)₆], [Ln(thd)₃] and [Ln(thd)₃(deta)], Ln = La, Sm, Gd. For each molecule gas phase geometry, vibrational spectrum and thermodynamic parameters have been calculated. Resulted molecular geometry agrees well with X-ray crystal structure, the corresponding Ln-N and Ln-O distances are equal within 0.05 Å (Tables S2, S3, S5). Calculated vibrational spectra also well correlate with experimental IR ones make it possible to perform the attribution of adsorption bands (Fig. 8, S7, S8).

In general, the sublimation process of mixed ligand complexes is described by the following reactions [19]:

$$Ln(thd)_3(deta)_{(s)} \leftrightarrow Ln(thd)_3(deta)_{(g)} \quad (5)$$

$$Ln(thd)_{3(s)} \leftrightarrow Ln(thd)_{3(g)} \quad (6)$$

$$Ln(thd)_{3(g)} \leftrightarrow 1/2Ln_2(thd)_{6(g)} \quad (7)$$

$$Ln(thd)_3(deta)_{(g)} \leftrightarrow Ln(thd)_{3(g)} + deta_{(g)} \quad (8)$$

$$Ln(thd)_3(deta)_{(g)} \leftrightarrow 1/2Ln_2(thd)_{6(g)} + deta_{(g)} \quad (9)$$

To estimate the relative stability of [Ln(thd)₃(deta)] complexes in the gas phase and to predict their behavior during sublimation the free energy changes of Eqs. (7)–(9) reactions have been calculated for room temperature and 433 K which corresponds to experimental evaporation condition (Table 3).

The free energy for dimerization of Ln(thd)₃ reaction (7) is negative only at room temperature being in agreement with crystal structure data of **1–5** which consist of binuclear [Ln₂(thd)₆] molecules. At higher temperature of the sublimation range (413–433 K), free energy change of (7) becomes noticeably positive making it possible to exclude reactions (7) and (9) from the consideration of sublimation processes.
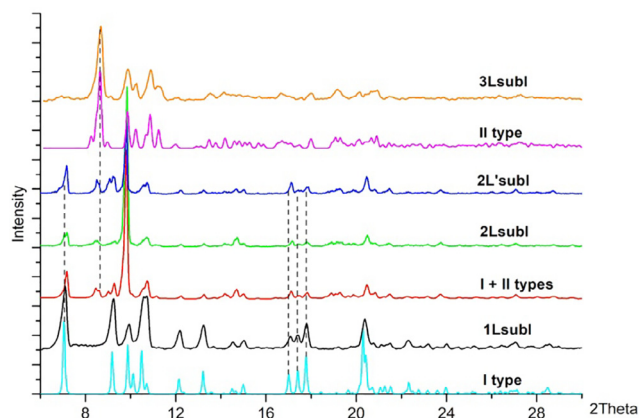
Fig. 7. Powder XRD patterns of sublimation products of La(thd)₃(deta) (**1Lsubl**), Pr(thd)₃(deta) (**2Lsubl**, **2L′subl**), Nd(thd)₃(deta) (**3Lsubl**); and theoretical patterns of La(thd)₃(deta) (**I type**), Sm(thd)₃(deta) (**II type**) and their mixture (**I + II types**). Significant deviation in intensities of **2L′subl** pattern originates from strong (1 0 0) texturing effect.
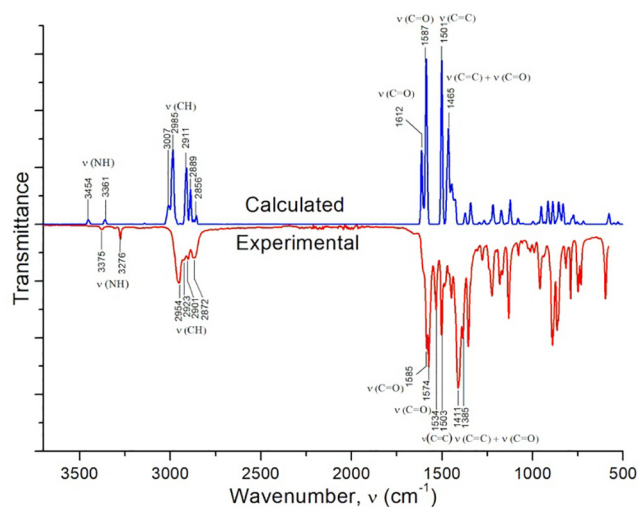
Fig. 8. Correlation of experimental (solid-state) and calculated (gas phase) IR spectra of [La(thd)₃(deta)].

Thus, reaction (8) is the most important. The change in the free energy of this reaction is positive for both temperatures (298 and 433 K), which shows the high stability of Ln(thd)₃(deta) complexes against the neutral ligand elimination, and one can expect to observe non-dissociated molecules in the gas phase, which is consistent with experimental data on identical compound compositions before and after sublimation. Going from La to Gd the positive charge density on central ion increases simultaneously with steric hindrances, these two counteracting factors cause non-uniform decrease of reaction (8) free energy change. Similar trend had been reported for Ln(thd)₃(Phen), where Ln-phen bonding energy was found to be 68.4 or 40.3 kJ/mol for Ln = La or Lu, respectively [54]. It should be noted that later values are smaller than calculated ΔE values for reaction (8) (Table 3).

3.5. MOCVD of LaMnO₃ and LaAlO₃ thin films

Thin films of textured (0 0 l) LaMnO₃ and (0 0 l) LaAlO₃ as well as (0 0 l) LaAlO₃/(0 0 l) LaMnO₃ heterostructure are considered to be optimal buffer layers for 2G high temperature superconductors [1,2]. MOCVD of these complex oxide thin films requires equal vapor pressure of precursors of each component. However, this could be hardly achieved due to quite different chemical properties of La, Mn and Al. Flash evaporator partially neglects the differences in volatility of precursors but optimization of precursors mixture composition is required. According to ICP-MS analysis of deposited LaMnO₃ films (Fig. S9) preparation of stoichiometric LaMnO₃ films from both precursors mixtures, **1 + 6** or **1L + 6**, requires remarkable excess of La compound in the initial precursor mixture. However **1L + 6** precursors mixture demonstrate more reproducible results with better linearity (Fig. S9). Obtained films on both MgO and SrTiO₃ substrates show single-phase (0 0 l) oriented LaMnO₃ XRD patterns (Fig. 9A). It is worth noting that large cell mismatch of LaMnO₃ and MgO results in appearance of polycrystalline LaMnO₃ admixture while perfect match between LaMnO₃ and SrTiO₃ cells leads to complete (0 0 l) peaks overlapping with no polycrystalline component.

Deposition of LaAlO₃ thin film by MOCVD is much more complex task due to its narrow cation homogeneity region, high melting point (2353 K) and drastic differences in volatility of La and Al precursors. The later issue can be overcomed by proper design of La precursor. We have performed deposition of LaAlO₃ film using **1L + 7** precursors mixture with different ratio La:Al equals to 1:2,

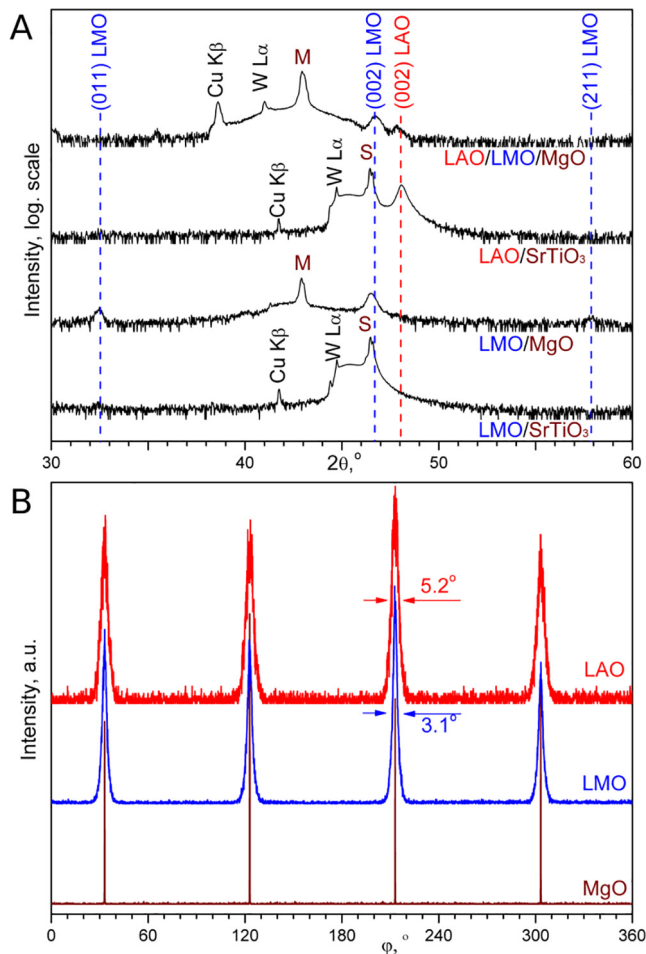**Fig. 9.** XRD patterns of LaAlO₃ (LAO) and LaMnO₃ (LMO) thin films obtained by MOCVD from **1L + 6** and **1L + 7** precursors mixtures on single crystalline (0 0 l) MgO (M) and (0 0 l) SrTiO₃ (S) substrates: symmetrical θ-2θ scans show phase composition and out-of-plane texture (A); φ-scans of (2 0 2) MgO, (1 0 1) LaMnO₃ and (1 0 1) LaAlO₃ reflexes for LaAlO₃/LaMnO₃/(0 0 l)MgO heterostructure show cube-on-cube in-plane texture, arrows show FWHM values of reflexes (B).

1:1 and 2:1. According to XRD data, equimolar mixture is optimal for deposition which leads to single-phase (0 0 l) oriented LaAlO₃ film with intense XRD pattern (Fig. 9A, Fig. S10). MOCVD with similar equimolar **1 + 7** mixture also leads to formation of (0 0 l) LaAlO₃ film but its XRD peaks are significantly less intense and much more wider which originates from low crystallinity of LaAlO₃ due to presence of amorphous impurities, e. g. Al₂O₃.

Finally, (0 0 l) LaAlO₃/(0 0 l) LaMnO₃/(0 0 l) SrTiO₃ and (0 0 l) LaAlO₃/(0 0 l) LaMnO₃/(0 0 l) MgO heterostructures have been successfully obtained by consequent MOCVD experiments using **1L + 6** and **1L + 7** precursors mixture. Both layers, LaAlO₃ and LaMnO₃, demonstrate cube-on-cube epitaxy with the following epitaxial relationships: (0 0 1)_LAO || (0 0 1)_LMO || (0 0 1)_MgO, [1 0 0]_LAO || [1 0 0]_LMO || [1 0 0]_MgO, (Fig. 9B). This demonstrates application of reported compounds as volatile precursors for complex oxide thin films, e. g. buffer layers for high-temperature coated conductors.

4. Conclusion

In this paper we report that coordination of tridentate deta ligand transforms binuclear [Ln(thd)₃]₂ (where Ln = La, Pr, Nd, Sm, Gd) to mononuclear mixed-ligand complex of identical composition [Ln(thd)₃(deta)] and similar molecular structure with

desirable coordination number equals to 9. Different polymorphic modifications were observed for structurally flexible [Ln(thd)$_3$(deta)] and even [La(thd)$_3$]$_2$ depending on synthetic conditions. Mixed ligand complexes [Ln(thd)$_3$(deta)], Ln = La, Pr, Nd, Sm sublime intact in temperature range of 140–160 °C and 0.01 Torr without decomposition. DFT calculations show [Ln(thd)$_3$(deta)] to be stable in the gas phase against ligand elimination, however, the stability decreases along with ionic radius that points to enhancement of steric hindrance in coordination sphere nine fold coordinated Ln^{3+} ion. Rather high stability of [Ln(thd)$_3$(deta)] in comparison to complexes with bidentate *N*-donor ligands and remarkable volatility of former ones at lower than [Ln(thd)$_3$]$_2$ temperatures allow them to be used as volatile precursors for MOCVD. [La(thd)$_3$(deta)] was successfully used for deposition of stoichiometric, single phase (0 0 l) oriented LaMnO$_3$ and LaAlO$_3$ thin films on (0 0 l) MgO and (0 0 l) SrTiO$_3$ substrates.

CRediT authorship contribution statement

Albina Nikolaeva: Visualization, Writing - original draft, Investigation. **Roy Nygaard:** Formal analysis, Investigation. **Irina Martynova:** Conceptualization, Investigation. **Dmitry Tsymbarenko:** Investigation, Conceptualization, Validation, Writing - review & editing, Supervision.

Acknowledgments

Appendix A. Supplementary data

CCDC (1950949, 1950801, 1950802, 1950803, 1975206) contains the supplementary crystallographic data the complexes **1**, **1L**, **4L**, **5L′** and **7**. These data can be obtained free of charge via http://www.ccdc.cam.ac.uk/conts/retrieving.html, or from the Cambridge Crystallographic Data Centre, 12 Union Road, Cambridge CB2 1EZ, UK; fax: (+44) 1223-336-033; or e-mail: deposit@ccdc.cam.ac.uk. Supplementary data to this article can be found online at https://doi.org/10.1016/j.poly.2020.114373.

References

[1] S. Samoilenkov, A. Molodyk, S. Lee, V. Petrykin, V. Kalitka, I. Martynova, A. Makarevich, A. Markelov, M. Moyzykh, A. Blednov, Supercond. Sci. Technol. 29 (2016), https://doi.org/10.1088/0953-2048/29/2/024001 024001.

[2] Y. Ma, K. Watanabe, S. Awaji, M. Motokawa, J. Cryst. Growth. 233 (2001) 483–489, https://doi.org/10.1016/S0022-0248(01)01587-1.

[3] G. Bellocchi, F. Fabbri, M. Miritello, F. Iacona, G. Franzo, ACS Appl. Mater. Interface 7 (2015) 18201–18205, https://doi.org/10.1021/acsami.5b05348.

[4] Y. Zhou, B. Yan, Nanoscale. 7 (2015) 4063–4069, https://doi.org/10.1039/C4NR06873D.

[5] V.V. Roddatis, A.R. Akbashev, S. Lopatin, A.R. Kaul, Appl. Phys. Lett. 103 (2013), https://doi.org/10.1063/1.4821044 112907.

[6] E. Coy, P. Graczyk, L. Yate, K. Załęski, J. Gapiński, P. Kuświk, S. Mielcarek, F. Stobiecki, B. Mróz, C. Ferrater, S. Jurga, Sci. Rep.-UK 7 (2017) 1–9, https://doi.org/10.1038/s41598-017-12370-y.

[7] W. Wang, J. Zhao, W. Wang, Z. Gai, N. Balke, M. Chi, H.N. Lee, W. Tian, L. Zhu, X. Cheng, D.J. Keavney, J. Yi, T.Z. Ward, P.C. Snijders, H.M. Christen, W. Wu, J. Shen, X. Xu, Phys. Rev. Lett. 110 (2013), https://doi.org/10.1103/PhysRevLett.110.237601 237601.

[8] R. Ramesh, N.A. Spaldin, Nat. Mater. 6 (2007) 21–29, https://doi.org/10.1038/nmat1805.

[9] M. Fiebig, T. Lottermoser, D. Meier, M. Trassin, Nat. Rev. Mater. 1 (2016), https://doi.org/10.1038/natrevmats.2016.46 16046.

[10] B. Hebler, A. Hassdenteufel, P. Reinhardt, H. Karl, M. Albrecht, ADV Mater. 3 (2016), https://doi.org/10.3389/fmats.2016.00008 8.

[11] Y. Hong, Z.G. Qiu, Z.G. Zheng, G. Wang, H.Y. Yu, D.Y. Chen, G.B. Han, D.C. Zeng, J. P. Liu, Acta Mater. 164 (2018) 627–635, https://doi.org/10.1016/j.actamat.2018.11.005.

[12] J.M.D. Coey, M. Viret, S. Molnár, Adv. Phys. 58 (2009) 571–697, https://doi.org/10.1080/000187399243455.

[13] H.O. Pierson, Handbook of Chemical Vapor Deposition (CVD): Principles, Technology and Applications, Noyes Publications, Park Ridge, N.J., USA, 1992.

[14] P.J. Wright, M.J. Crosbie, P.A. Lane, D.J. Williams, A.C. Jones, T.J. Leedham, H.O. Davies, J. Mater. Sci.-Mater. Elem. 13 (2002) 671–678, https://doi.org/10.1023/A:1020618411750.

[15] E.M. Aisen, V.D. Borisevich, E.V. Levin, G.E. Popov, A.V. Tikhomirov, S.V. Yupatov, Nucl. Instrum. Methods Sect. A 374 (1996) 127–131, https://doi.org/10.1016/0168-9002(96)00065-4.

[16] S. Shahbazi, C.J. Oldham, A.D. Mullen, J.D. Auxier II, H.L. Hall, Radiochim. Acta 107 (2019) 1173–1184, https://doi.org/10.1515/ract-2018-3085.

[17] R.D. Teo, J. Termini, H.B. Gray, J. Med. Chem. 59 (2016) 6012–6024, https://doi.org/10.1021/acs.jmedchem.5b01975.

[18] M. Tiitta, L. Niinistou, Chem. Vap. Deposition 3 (1997) 167–182, https://doi.org/10.1002/cvde.19970030404.

[19] A. Drozdov, N. Kuzmina, in: Comprehensive Inorganic Chemistry II, J. Reedijk, K. Poeppelmeier (Eds.), Elsevier, USA, 2013, pp. 511–534.

[20] C.S. Erasmus, J.C.A. Boeyens, Acta Crystallogr., Sect. B: Struct. 26 (1970) 1843–1854, https://doi.org/10.1107/S0567740870004983.

[21] A.F. Kirby, R.A. Palmer, Inorg. Chem. 20 (1981) 1030–1033, https://doi.org/10.1021/ic50218a016.

[22] A. Lennartson, M. Vestergren, M. Håkansson, Chem. Eur. J. 11 (2005) 1757–1762, https://doi.org/10.1002/chem.200401019.

[23] K. Yanagisawa, Y. Kitagawa, T. Nakanishi, T. Akama, M. Kobayashi, T. Seki, K. Fushimi, H. Ito, T. Taketsugu, Y. Hasegawa, Eur. J. Inorg. Chem. 32 (2017) 3843–3848, https://doi.org/10.1002/ejic.201700815.

[24] K. Binnemans, Handbook on the Physics and Chemistry of Rare Earths, Elsevier, USA, 2005, p. 35.

[25] I. Baxter, S.R. Drake, M.B. Hursthouse, K.M.A. Malik, J. McAleese, D.J. Otway, J.C. Plakatouras, Inorg. Chem. 34 (1995) 1384–1394, https://doi.org/10.1021/ic00110a016.

[26] G. Malandrino, C. Benelli, F. Castelli, I.L. Fragala, Chem. Mater. 10 (1998) 3434–3444, https://doi.org/10.1021/cm980172j.

[27] G. Malandrino, O. Incontro, F. Castelli, I.L. Fragala, C. Benelli, Chem. Mater. 8 (1996) 1292–1297, https://doi.org/10.1021/cm950569c.

[28] D. Grebenyuk, N. Ryzhkov, D. Tsymbarenko, J. Fluorine Chem. 202 (2017) 82–90, https://doi.org/10.1016/j.jfluchem.2017.08.014.

[29] W. Tang, R. Chen, J. Zhao, W. Jiang, Y. Zhang, D. Jia, CrystEngComm 14 (2012) 5021–5026, https://doi.org/10.1039/C2CE25135C.

[30] J. Zhou, X.-H. Yin, F. Zhang, CrystEngComm 13 (2011) 4806–4809, https://doi.org/10.1039/C1CE05314K.

[31] D. Grebenyuk, I. Martynova, D. Tsymbarenko, Eur. J. Inorg. Chem. 2019 (2019) 3103–3111, https://doi.org/10.1002/ejic.201900643.

[32] P. Magnus, A.H. Payne, M.J. Waring, D.A. Scott, V. Lynch, Tetrahedron Lett. 41 (2000) 9725–9730, https://doi.org/10.1016/S0040-4039(00)01727-5.

[33] G.S. Hammond, W.G. Borduin, G.A. Guter, J. Am. Chem. Soc. 81 (1959) 4682–4686.

[34] P.A. Stabnikov, A.I. Smolentsev, N.V. Pervukhina, O.S. Koshcheeva, L.N. Komissarova, S.V. Borisov, J. Struct. Chem. 52 (2011) 118–124, https://doi.org/10.1134/S0022476611010161.

[35] N.V. Belova, B. Dalhus, G.V. Girichev, N.I. Giricheva, A. Haaland, N.P. Kuzmima, T.A. Zhukova, J. Struct. Chem. 22 (2011) 393–399, https://doi.org/10.1007/s11224-010-9729-0.

[36] M.A.K. Ahmed, H. Fjellvåg, A. Kjekshus, D.S. Wragg, Z. Anorg. Allg. Chem. 639 (2013) 770–778, https://doi.org/10.1002/zaac.201200478.

[37] G.M. Sheldrick, SADABS v.2.01, Bruker/Siemens Area Detector Absorption Correction Program, Bruker AXS, Madison, Wisconsin, USA, 1998.

[38] W. Kabsch, XDS, Acta Crystallogr., Sect. D 66 (2010) 125–132, https://doi.org/10.1107/S0907444909047337.

[39] G.M. Sheldrick, SHELXTL. Version 5.10. Structure Determination Software Suite, Bruker AXS, Madison, 1998.

[40] A.A. Granovsky, Firefly Version 8.2, http://classic.chem.msu.su/gran/firefly/index.html. (Accessed 5 September 2019).

[41] Stuttgart/Cologne energy-consistent (ab initio) pseudopotentials, http://www.tc.uni-koeln.de/PP/index.en.html. (Accessed 5 September 2019).

[42] S.F. Boys, F. Bernardi, Mol. Phys. 19 (1970) 553–566, https://doi.org/10.1080/00268977000101561.

[43] A.A. Bossak, I.E. Graboy, O.Yu. Gorbenko, A.R. Kaul, M.S. Kartavtseva, V.L. Svetchnikov, H.W. Zandbergen, Chem. Mater. 16 (2004) 1751–1755, https://doi.org/10.1021/cm0353660.

[44] P.A. Stabnikov, S.A. Mosyagina, K.V. Zherikova, I.V. Korolkov, N.V. Pervukhina, N.B. Morozova, J. Struct. Chem. 58 (2017) 1693–1696, https://doi.org/10.1134/S0022476617080327.

[45] L. Yuikhan, S.A. Mosyagina, P.A. Stabnikov, N.I. Alferova, I.V. Korol'kov, N.V. Pervukhina, N.B. Morozova, J. Struct. Chem. 58 (2017) 843–846, https://doi.org/10.1134/S0022476617040333.

[46] P.A. Stabnikov, I.V. Korol'kov, N.V. Pervukhina, O.V. Antonova, P.E. Plyusnin, S. A. Prokhorova, S.V. Larionov, Russ. J. Gen. Chem. 85 (2015) 135–143, https://doi.org/10.1134/S1070363215010235.

[47] R.C. Holz, L.C. Thompson, Inorg. Chem. 32 (1993) 5251–5256, https://doi.org/10.1021/ic00075a051.

[48] A. Kitaigorodsky, Molecular Crystals and Molecules, 1st ed., Academic Press, London, 1973.

[49] R.C. Holz, L.C. Thompson, Inorg. Chem. 27 (1988) 4640–4644, https://doi.org/10.1021/ic00298a027.

[50] S.R. Drake, A. Lyons, D.J. Otway, A.M.Z. Slawin, D.J. Williams, J. Chem. Soc. Dalton. 15 (1993) 2379–2386, https://doi.org/10.1039/DT9930002379.

[51] J.C. Plakatouras, C. Kavounis, C.J. Cardin, Acta Crystallogr., Sect. E 59 (2003) m838–m840, https://doi.org/10.1107/S1600536803016556.

[52] R.L. Nigro, R.G. Toro, M.E. Fragala, P. Rossi, P. Dapporto, G. Malandrino, Inorg. Chim. Acta. 362 (2009) 4623–4629, https://doi.org/10.1016/j.ica.2009.05.044.

[53] W.J. Evans, D.G. Giarikos, M.A. Johnston, M.A. Greci, J.W. Ziller, J. Chem. Soc. Dalton. (2002) 520–526, https://doi.org/10.1039/B104095M.

[54] A.V. Nemukhin, A.Y. Rogachev, S.V. Konyukhov, A.V. Bochenkova, A.A. Granovsky, Int. J. Quantum Chem. 104 (2005) 203–213, https://doi.org/10.1002/qua.20412.